ACS OMEGA

http://pubs.acs.org/journal/acsodf

Article

Effects of Local Sequence, Reaction Conditions, and Various Additives on the Formation and Stability of Interstrand Cross-Links Derived from the Reaction of an Abasic Site with an Adenine Residue in Duplex DNA

Saosan Binth Md. Amin, Tanhaul Islam, Nathan E. Price, Amanda Wallace, Xu Guo, Anuoluwapo Gomina, Marjan Heidari, Kevin M. Johnson, Calvin D. Lewis, Zhiyu Yang, and Kent S. Gates*

Cite This: *ACS Omega* 2022, 7, 36888−36901

Read Online

ACCESS | Metrics & More | Article Recommendations | Supporting Information

ABSTRACT: The experiments described here examined the effects of reaction conditions, various additives, and local sequence on the formation and stability interstrand cross-links (ICLs) derived from the reaction of an apurinic/apyrimidinic (AP) site with the exocyclic amino group of an adenine residue on the opposing strand in duplex DNA. Cross-link formation was observed in a range of different buffers, with faster formation rates observed at pH 5. Inclusion of the base excision repair enzyme alkyladenine DNA glycosylase (hAAG) which binds tightly to AP-containing duplexes decreased, but did not completely prevent, formation of the dA-AP ICL. Formation of the dA-AP ICL was not altered by the presence of the biological metal ion Mg^{2+} or the biological thiol, glutathione. Several organocatalysts of imine formation did not enhance the rate of dA-AP ICL formation. Duplex length did not have a large effect on dA-AP yield, so long as the melting temperature of the duplex was not significantly below the reaction temperature (the duplex must remain hybridized for efficient ICL formation). Formation of the dA-AP ICL was examined in over 40 different sequences that varied the neighboring and opposing bases at the cross-linking site. The results indicate that ICL formation can occur in a wide variety of sequence contexts under physiological conditions. Formation of the dA-AP ICL was strongly inhibited by the aldehyde-trapping agents methoxyamine and hydralazine, by $NaBH_3CN$, by the intercalator ethidium bromide, and by the minor groove-binding agent netropsin. ICL formation was inhibited to some extent in bicarbonate and Tris buffers. The dA-AP ICL showed substantial inherent stability under a variety of conditions and was not a substrate for AP-processing enzymes APE1 or Endo IV. Finally, we characterized cross-link formation in a small (11 bp) stem-loop (hairpin) structure and in DNA-RNA hybrid duplexes.

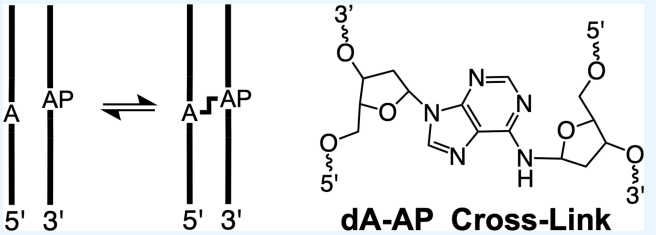

INTRODUCTION

Apurinic/apyrimidinic (AP) sites arise by spontaneous and enzyme-catalyzed hydrolysis of the carbon−nitrogen bonds connecting nucleobases to the deoxyribose backbone.[1−5] and are among the most common unavoidable lesions generated in DNA.[6,7] Importantly, AP sites in duplex DNA exist as a mixture of the ring-closed hemiacetal and the ring-opened aldehyde.[8] Reaction of the AP aldehyde with the exocyclic amino groups of nucleobases on the opposing strand can generate interstrand cross-links (ICL).[9−12] A group of AP-derived ICLs involving both canonical and noncanonical nucleobases have been characterized over the last 15 years.[13−20]

The formation of AP-derived ICLs proceeds via initial generation of an imine (Schiff base) intermediate followed by cyclization of the C4-hydroxyl group onto the C1-carbon of the imine to yield a stable aminoglycoside cross-link (Figure 1A).[21−23] In the case of nucleobases that position an NH_2 group in the minor groove (guanine or 2-aminopurine), cross-link formation is favored in sequence motifs where the nucleobase is located one nucleotide to the 5′-side of the AP site (e.g., 5′CX/5′NG, where X = AP site and N = any nucleobase, Figure 1B).[13,15,18] On the other hand, for nucleobases that position an NH_2 group in the major groove (adenine, cytosine, N^4-aminocytosine), ICL formation is favored in sequence motifs where the cross-linked nucleobase is offset one nucleotide to the 3′-side of the AP site on the

Received: September 4, 2022
Accepted: September 28, 2022
Published: October 4, 2022

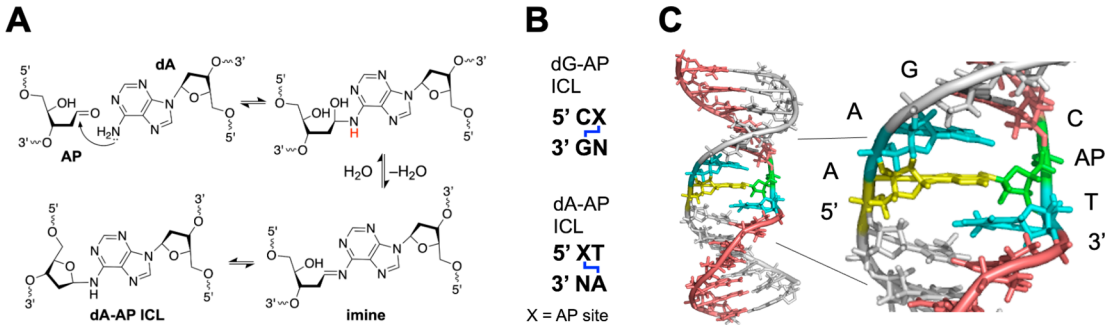

Figure 1. dA-AP ICL. (A) Formation mechanism for the dA-AP ICL. (B) Sequence motifs for the dG-AP and dA-AP ICLs. (C) Structure of the dA-AP ICL in duplex DNA. Image prepared from pdb code 6xah using Pymol.

1a 5′ATACCAGATAGATGGA **CXT** AGACATATACACAGAT
3′TATGGTCTATCTACTT **GAA** TCTGTATATGTGTCTA

1b 5′AGATAGATGAA **CXT** AGACATATACA
3′TCTATCTACTT **GAA** TCTGTATATGT

1c 5′ATAGATGAA **CXT** AGACATAT
3′TATCTACTT **GAA** TCTGTATA

1d 5′GATGAA **CXT** AGACAT
3′CTACTT **GAA** TCTGTA

1e 5′TGAA **CXT** AGA
3′ACTT **GAA** TCT

X= AP site or AP site in dA-AP ICL
⌙ indicates site of ICL attachment

2 5′ATACCAGTTATACAAT **GXT** GTTCTAATTCACAGAT
3′TATGGTCAATATGTTA **CAA** CAAGATTAAGTGTCTA

3 5′ATAGGACATCGAGATT **TXA** CTGTAGCTAATTTGAT
3′TATCCTGTAGCTCTAA **AGA** GACATCGATTAAACTA

4/5 5′TTTTTTTTTTTTTTTT **CXT** TTTTTTTTTTTTTTTT
3′TTTTTTTTTTTTTTTT **GAA** TTTTTTTTTTTTTTTT

6 5′TCTAATTCACAGTTTTACGACTTATACAAT **GXT** GT
3′AGATTAAGTGTCAAAATGCTGAATATGTTA **CAA** CA
36±3%

7 5′TTCTAATTCACAGTTTTACGACTTATACAAT **GXT** G
3′AAGATTAAGTGTCAAAATGCTGAATATGTTA **CAA** C
23±2%

8 5′TTACGACTTATACAAT **GXT** GTTCTAATTCACAGTT
3′AATGCTGAATATGTTA **CAA** CAAGATTAAGTGTCAA
19±5%

Figure 2. DNA sequences used in this study.

opposing strand (e.g., 5′XT/5′AN, where X = AP site and N = any nucleobase, Figure 1B).[14,16,17]

The sequence motifs for the formation of AP-derived ICLs are a consequence of the right-handed helical twist of B-form DNA.[18,24] NMR structural analysis of a DNA duplex containing the dA-AP ICL shows how the helical twist of DNA positions the major groove NH_2 group of the cross-linking adenine residue proximal to C1 of the AP site, thereby enabling ICL formation without energetically costly distortions of the duplex structure (Figure 1C).[21] As a result, the cross-linked duplex retains a largely B-helical structure with only modest unwinding near the ICL. The cross-linked adenine residue is unpaired and the resulting orphan thymine residue retains stacking interactions with its 3′-neighbor while gaining stacking interactions on its 5′-face with the cross-linked adenine (its former base-pairing partner). The 5′AAG sequence (in which the underlined A is cross-linked) opposing the AP site forms a well-stacked run of purines.[21]

Given the ubiquitous nature of AP sites in DNA and the fact that ICLs block the read out of genetic information, AP-derived ICLs might be important lesions. Among the canonical nucleobases, adenine residues generate the highest equilibrium ICL yields.[13−18] Recent identification of a eukaryotic pathway that the repairs dA-AP ICL adds further biological motivation to fully characterize the properties of this lesion.[25−28] In the work described here, we examined formation and stability of the dA-AP ICL in a wide variety of sequences and under a wide variety of reaction conditions.

RESULTS AND DISCUSSION

Generation of AP-Containing DNA Duplexes and Detection of dA-AP ICLs Using Gel Electrophoresis. DNA duplexes containing an AP site at a defined location were generated by treatment of the corresponding 2′-deoxyuridine-containing duplex with uracil DNA glycosylase (UDG).[15,29−31] In most experiments, the dU-containing strand (and, thus, the resulting AP-containing strand) was labeled on the 5′-end with either a ^{32}P phosphoryl group or a Cy5 fluorophore to enable detection of the products generated under various conditions. The labeled products were resolved by electrophoresis on a denaturing 20% polyacrylamide gel and visualized by storage phosphor autoradiography or fluorescence imaging.[32]

Generation of the AP site was confirmed by treatment of the oligodeoxynucleotide with NaOH or piperidine to generate fast-migrating labeled cleavage products with 3′-phosphoryl (3′P), 3′-unsaturated phosphoaldehyde (3′-PUA), or 3′-deoxyribose (3′dR) termini.[33−35] Duplexes containing an AP-derived ICL migrate slowly in denaturing gels, appearing near the top of the images shown here.[13−18] In some reactions, a minor band corresponding to a second type of cross-linked DNA duplex can be seen migrating slightly faster than the full-size dA-AP cross-link. Our previous work indicates that this band corresponds to an ICL derived from strand cleavage at the AP site.[19,20,36] Many of the studies reported here were carried out using one of three "core cross-linking sequences" **1**−**3**, in which the formation of the dA-AP ICL has been characterized previously (Figure 2).[14,22,36,37] Sequence **1** contains both dA-AP and dG-AP cross-linking motifs, but

https://doi.org/10.1021/acsomega.2c05736
ACS Omega 2022, 7, 36888−36901

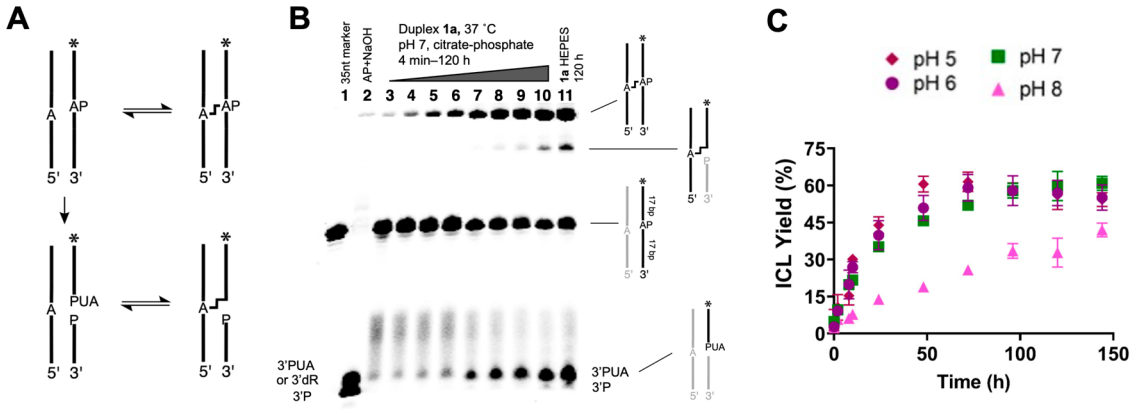

Figure 3. Gel electrophoretic analysis of dA-AP ICL formation. (A) Schematic diagram depicting the formation of AP-derived ICLs. In addition to cross-linking of the intact AP site (upper right), the diagram depicts formation of a cross-linked species (lower right) derived from spontaneous cleavage of the AP site.(B) Representative example of gel electrophoretic analysis of ICL formation in duplex **1a** incubated in McIlvane's phosphate–citrate buffer at pH 7. The AP-containing strand was labeled on the 5′-end with a fluorescent Cy5 dye. Lane 1: 35 nt size marker. Lane 2: treatment of the AP-containing duplex with NaOH to generate 3′phosphate, 3′PUA, or 3′dR cleavage products.[34] Lanes 3–10: incubation of AP-containing duplex **1a** in pH 7 phosphate–citrate buffer, incubated at 37 °C for varying times. Lane 11: comparison reaction showing formation of cross-linked and cleavage products resulting from the incubation of duplex **1a** in HEPES buffer (50 mM, pH 7.4 containing 100 mM NaCl) for 120 h. The resulting DNA products were resolved in a denaturing 20% polyacrylamide gel and visualized by fluorescence imaging. The gray segments in the duplex cartoons shown on the right side of the gel image are not labeled and, therefore, cannot be seen in the gel image. (C) Plots showing the time-courses for the formation of dA-AP ICL in duplex **1a** incubated in phosphate–citrate buffer at pH values of 5, 6, 7, and 8.

previous studies have shown the only detectable cross-link formed in this sequence is the dA-AP ICL.[14,21]

Effects of Buffers and pH on Formation of the dA-AP ICL. In most previous studies, formation of the dA-AP ICL was carried out in HEPES buffer (50 mM, pH 7.4) containing 100 mM NaCl.[14,22,36−38] Here we examined time-courses for cross-link formation in several different buffers and at pH values between 5 and 8.

We measured formation of the dA-AP ICL in the AP-containing duplex **1a** at pH values of 5, 6, 7, and 8 in a universal phosphate–citrate buffer system (McIlvane's buffer, Figure 3).[39] The rate of ICL formation was somewhat faster at pH 5, reaching its half-maximal yield within approximately 12 h and maximal yields around 50 h. At pH 7, the cross-linking reaction reached its half-maximal yield at about 24 h and maximum yield at about 75 h. The formation rate was significantly lower at pH 8, and the reaction does not appear to have reached a final equilibrium yield even after 150 h (Figure 3C and Table 1).

We also examined formation of the dA-AP ICL in three different AP-containing duplexes **1a**, **2**, and **3** in phosphate-buffered saline (50 mM sodium phosphate, 100 mM NaCl) at pH 6, 7, and 8 (Figure S1). The yields of ICL formation followed the trend **3** > **1a** > **2**, consistent with our published results for these sequences.[14,22,36,37] The pH effects on the rate of ICL formation in duplex **1a** mirrored the results described above for ICL formation in phosphate–citrate buffer, showing faster cross-link formation at pH 6 and 7 and slower cross-link formation at pH 8. In duplexes **2** and **3**, we observed more striking pH effects, with the rate of ICL formation displaying the trend pH 6 > pH 7 > pH 8. These results are generally consistent with chemical precedents showing that the rates of imine formation are greater pH values near 5.[40]

Bicarbonate/CO_2 is an important component of the intracellular pH buffering system.[41] The intracellular concentration of bicarbonate is in the range of 20 mM.[41,42] Therefore, we examined whether bicarbonate buffer alters formation of the dA-AP ICL. We found that the dA-AP ICL forms when duplex **1a** is incubated in bicarbonate buffer (50 mM) containing NaCl (100 mM) at pH values of 6, 7, and 8, although, interestingly, the yields were approximately 2-fold lower than those observed in the other buffers examined here (Figures 4 and S2). The mechanistic basis for the bicarbonate effect on the yield of dA-AP ICL remains unclear. It is possible that the exocyclic amino group of adenine reacts reversibly

Table 1. Effects of Buffers and Various Additives on the Rate of ICL Formation in Duplex 1a at 37 °C

Buffer	Half time to completion (h) **1**
HEPES and NaCl; pH 7.4	24
Phosphate and NaCl; pH 6	12
Phosphate and NaCl; pH 7	24
Phosphate and NaCl; pH 8	>48
Phosphate and $MgCl_2$; pH 6	8
Phosphate and $MgCl_2$; pH 7	8
Phosphate and $MgCl_2$; pH 8	>24
Buffer	**Half time to completion (h)**
Citrate–phosphate and NaCl; pH 5	10
Citrate–phosphate and NaCl; pH 6	12
Citrate–phosphate and NaCl; pH 7	24
Citrate–phosphate and NaCl; pH 8	>48
Citrate–phosphate and $MgCl_2$; pH 5	8
Bicarbonate and NaCl; pH 6	12
Bicarbonate and NaCl; pH 7	24
Tris and NaCl; pH 7	12
Sodium acetate and NaCl; pH 5	8
Sodium acetate and $MgCl_2$; pH 5	8
Additive	**Half time to completion (h)**
HEPES and NaCl; pH 7.4 (std buffer)	24
Std buffer + anthranilic acid	24
Std buffer + aniline	24
Std buffer + DMEDA	24
Std buffer + GSH	24
Std buffer + guanidine·HCl	36
Std buffer + L-arginine	48

https://doi.org/10.1021/acsomega.2c05736
ACS Omega 2022, 7, 36888−36901

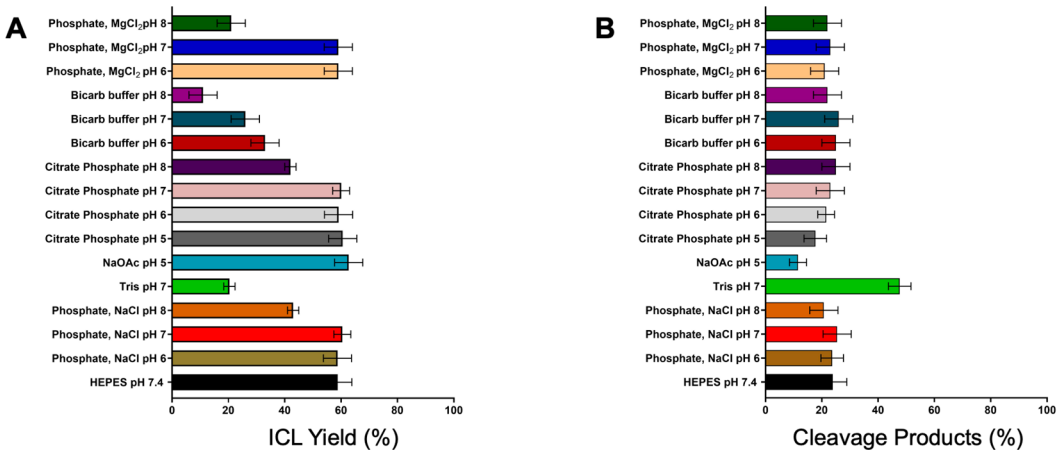

Figure 4. Buffer and pH effects on the formation of dA-AP ICL in duplex **1a**. (A) ICL yield after 120 h at 37 °C in the specified buffer. Details of buffer and salt concentrations for each condition are provided in the text. (B) Amount of strand cleavage that accompanies ICL formation after 120 h at 37 °C.

with CO_2 to generate equilibrium amounts of a carbamic acid derivative that is incapable of cross-linking (for analogous reactions of NH_2 groups with CO_2 see refs 43 and 44).

We also observed a lower ICL yield in Tris buffer (pH 7.4) compared to the other buffers examined here. In this case, the decreased ICL yield was accompanied by an increase in strand cleavage at the AP site in duplex **1a** (Figure 4). The amine group of Tris buffer can react with aldehyde functional groups,[45−47] and we suggest that conversion of the AP aldehyde residue to a Tris-derived iminium ion induces cleavage of the AP site at the expense of ICL formation (Figures 4 and S3).[34,48,49]

Overall, we observed significant pH effects on the rate of ICL formation, with lower pH values (pH 5−6) supporting faster formation rates. We did not observe large pH effects on the final, equilibrium yields of ICL formation. In many cases, we did not observe significant effects exerted by buffer salts. For example, the rates and yields of ICL formation measured for duplex **1a** in pH 5 sodium acetate buffer were similar to those observed in pH 5 phosphate−citrate buffer (Figure 4, Table 1) and the rates and yields of ICL formation in pH 7.4 HEPES buffer, pH 7 phosphate−citrate buffer, and pH 7 phosphate−NaCl were similar (Figure 4, Table 1). In contrast, bicarbonate buffer and Tris buffers diminished the yields of dA-AP ICL generated in the AP-containing duplex **1a**.

Formation of the dA-AP ICL Occurs in the Presence of the Biological Metal Ion Mg^{2+} and the Biological Thiol Glutathione. The cellular environment contains magnesium ions that can significantly alter the stability and dynamics of duplex DNA.[50] In addition, magnesium ions can catalyze imine formation in organic solvents.[51] Accordingly, we examined whether magnesium ions affect formation of the dA-AP ICL.

We found that inclusion of $MgCl_2$ (2 mM) slightly increased the rate of dA-AP ICL formation in duplex **1a** in pH 6 or 7 sodium phosphate buffer (50 mM, Figures S1A and S4A). Under these conditions, the half-maximal yield of ICL was achieved within 8 h (Table 1 and Figure S4A). Similarly, ICL formation was slightly faster in HEPES buffer (50 mM, pH 7.4) containing 2 mM $MgCl_2$ compared to the same buffer containing 100 mM NaCl (Figure 4 and S4B).

Cells contain millimolar concentrations of the thiol-containing tripeptide glutathione (GSH).[52,53] Thiol groups can add reversibly to aldehydes,[54] and in some cases, this can alter the rate of imine formation.[55] In addition, recent studies provided evidence that glutathione can form a thioglycoside adduct with an AP site in DNA, a process that potentially could inhibit formation of AP-derived ICLs.[56]

We found that inclusion of glutathione (2−5 mM) did not substantially alter the rate or yield of ICL formation when the AP-containing duplex **1a** was incubated in HEPES buffer (50 mM, pH 7.4, 100 mM NaCl) (Figure S4C). The results indicate that the physiological metal ion, Mg^{2+}, and the biological thiol, glutathione, are compatible with formation of the dA-AP ICL.

Organocatalysts of Imine Formation Do Not Increase the Rate of dA-AP ICL Formation. Formation of AP-derived ICLs likely proceeds via an imine intermediate (Figure 1A). Therefore, we examined whether inclusion of established imine-formation catalysts aniline (1 mM),[57,58] anthranilic acid (100 mM),[59] arginine (1 mM),[60] and *N,N′*-dimethylethylenediamine (DMEDA, 20 mM)[61] increased the rate of ICL formation in the AP-containing duplex **1a**. We found that none of these agents served as effective catalysts for dA-AP cross-link formation (Table 1). In the cases of aniline, guanidine, and DMEDA, the additives decreased the ICL yield to less than 20% (approximately 3-fold decrease in yield). In the case of aniline, the decreased the yield of may be due to competitive formation of a stable arylaminoglycoside adduct.[62] *N,N′*-Dimethylethylenediamine decreased the ICL yield because the AP site was converted to strand cleavage products at the expense of dA-AP ICL formation (Figure S5). This was not surprising in light of the existing literature describing amine-catalyzed cleavage of AP sites in DNA.[34,63] Arginine decreased the rate of ICL formation. Anthranilic acid had no significant effect on ICL formation.

Length of the AP-Containing Duplex Does Not Dramatically Affect Yield of the dA-AP ICL unless the Reaction Temperature Is Substantially above the Melting Temperature of the Duplex. We examined whether the length of the AP-containing duplex had any effect on the yield of dA-AP ICL. A series of duplexes (**1a**−**e**) with the same core cross-linking sequence found in **1a** were incubated in HEPES pH 7.4 buffer (50 mM) containing 100 mM NaCl at 37 °C. We observed the following trend for the cross-link yield in AP-containing duplexes of varied length: 35

https://doi.org/10.1021/acsomega.2c05736
ACS Omega 2022, 7, 36888−36901

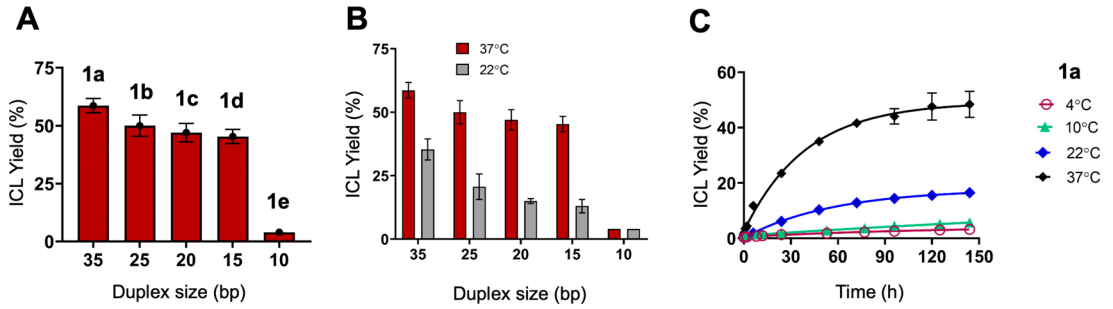

Figure 5. Effects of duplex length and reaction temperature on formation of the dA-AP ICL. Reactions were carried out in HEPES buffer (50 mM, pH 7.4 containing 100 mM NaCl). (A) Duplex length does not have a large effect on ICL yield, so long as the T_m of the duplex is not significantly below reaction temperature (37 °C, in this case). The calculated melting temperatures of the duplexes are **1a** 56 °C, **1b** 48 °C, **1c** 42 °C, **1d** 35 °C, and **1e** 15 °C. (B) Compared to 22 °C. C. Formation of the dA-AP ICL in duplex **1a** at 4, 10, 22, and 37 °C. The final, equilibrium yield of ICL was greater at 37 °C than 22 °C.

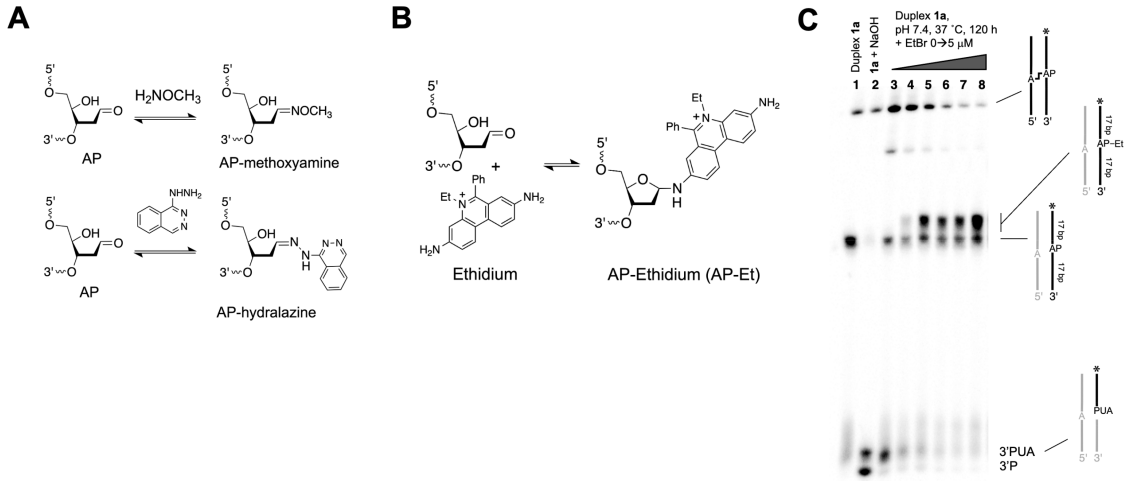

Figure 6. Covalent capture of the AP site inhibits formation of the dA-AP ICL. (A) Reactions of methoxyamine and hydralazine with an AP site in duplex DNA. (B) Proposed reaction of ethidium bromide with an AP site in DNA. (C) Ethidium bromide inhibits formation of the dA-AP ICL in duplex **1a**, with accompanying formation of a covalent adduct with the AP site. The cross-linking reaction was carried out in HEPES buffer (50 mM, pH 7.4 containing 100 mM NaCl). In the reactions analyzed in lanes 3−8, the AP-containing duplex was incubated for 120 h with 0, 0.1, 0.5, 1, 2, or 5 μM ethidium bromide, respectively.

nt >25 nt >20 nt >15 nt (Figure 5A). Importantly, the differences in the ICL yields among duplexes **1a**−**e** were modest. On the other hand, we obtained a very low yield of ICL in a reaction containing the complementary oligonucleotides **1e**, likely because the 10 nt AP-containing duplex derived from these short DNA fragments does not remain hybridized at the reaction temperature of 37 °C (the melting temperature of this AP-containing duplex is estimated at 15 °C). Similarly, we observed no slow-migrating, cross-linked DNA bands in the gel when the largely noncomplementary oligodeoxynucleotides **4** and **5** were incubated in HEPES pH 7.4 buffer for 120 h at 37 °C (Figure S6).

We found that good ICL yields were obtained when the cross-linking motif was located near the ends of duplexes **6** and **7** (Figure 2). In fact, the ICL yield was greater in duplex **6**, in which the cross-linking motif is located near the end, compared to the same three-nucleotide cross-linking sequence located in the middle of duplex **8** (yields are shown in Figure 2). The results suggest that increased duplex dynamics[64] on the 3′-side of the AP site facilitate the structural reorganizations associated with formation of the dA-AP ICL (we have not examined duplexes in which the 5′-side of the AP site is near the end of the duplex). These results are generally consistent with our previous observation that dA-AP ICLs can be formed near the junction of duplex−single-strand regions.[27]

Effect of Temperature on the Yield of dA-AP ICL. The AP-containing duplexes **1a**−**d** (35, 25, 20, and 15 nt in length) were incubated for 120 h in HEPES buffer (50 mM, pH 7.4, containing 100 mM NaCl) at either 37 or 22 °C (Figure 5B). ICL yields were higher at 37 °C than at 22 °C (the 10 nt duplex **1e** gave low ICL yields at both 37 and 22 °C). To further investigate the effects of temperature on formation of the dA-AP ICL, we measured the time courses for ICL formation in the 35 nt AP-containing duplex **1a** at 4, 10, 22, and 37 °C (Figure 5C). The ICL yields at 4 and 10 °C were low. On the other hand, the reactions carried out at 22 and 37 °C both gave substantial yields of ICL and appear to have reached equilibrium by 145 h. The ICL yield at 37 °C was approximately 3 times greater than the yield at obtained at 22 °C. The temperature dependence suggests a positive entropy of reaction for formation of the dA-AP ICL in duplex **1a**.

Formation of the dA-AP ICL Is Inhibited by the Aldehyde-Trapping Reagents Methoxyamine and Hydralazine, by the DNA Intercalator Ethidium Bromide, and by the Minor Groove Binding Agent Netropsin. We surveyed some potential inhibitors of dA-AP ICL formation. We first validated our previous observation[14] that inclusion of

https://doi.org/10.1021/acsomega.2c05736
ACS Omega 2022, 7, 36888−36901

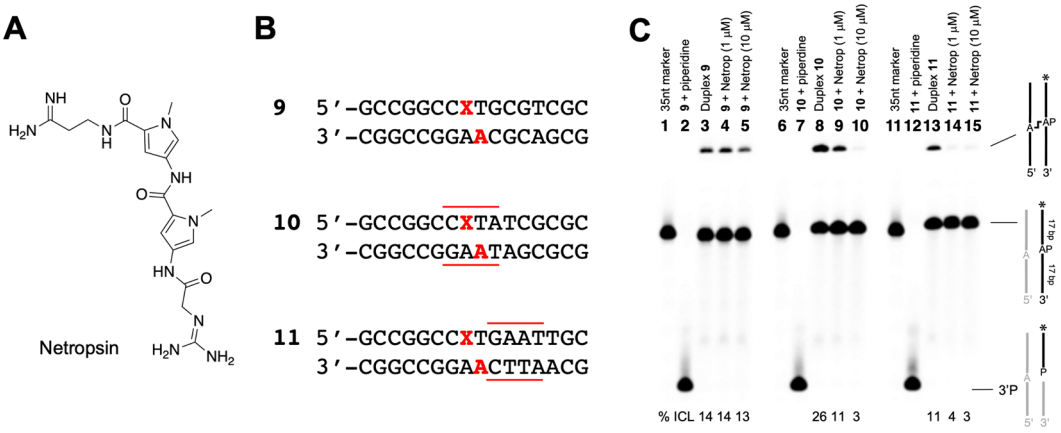

Figure 7. Noncovalent binding of netropsin to duplexes **10** and **11** inhibits formation of the dA-AP ICL. (A) Structure of the minor groove binding agent netropsin. (B) Sequences used in the netropsin experiments. The red letters indicate the cross-linking site in **9** and the expected cross-linking sites in **10** and **11**. The red lines indicate A/T-rich netropsin binding sites. The dissociation constants for netropsin complexed with A/T-rich sequences of duplex DNA are in the range of 8−100 nM.[80,81] (C) Gel electrophoretic analysis showing that netropsin binding inhibits dA-AP ICL formation. The reactions were incubated for 120 h at 37 °C in HEPES buffer (50 mM, pH 7 containing 100 mM NaCl). The ICL yields have a standard deviation of less than ±10%. Cleavage of the AP-containing duplex to verify successful generation of the AP site (lanes 2, 7, 12) was carried out by treatment with warm piperidine (1 M, 60 °C, 30 min).

the aldehyde-trapping reagent methoxyamine (2 mM) completely prevented formation of the ICL in duplex **1a** by competitive conversion of the AP aldehyde residue to the corresponding oxime derivative (Figures 6A and S7).[65,66] Similarly, we showed that the antihypertensive agent hydralazine (100 μM) blocked ICL formation in duplex **1a** (Figure S7). Inhibition of ICL formation by hydralazine involves efficient conversion of AP sites in duplex DNA to the hydrazone adduct (Figure 6A).[67] The semicarbazide-containing drug isoniazid (40 μM) did not inhibit formation rate or yield of dA-AP ICL formation in duplex **1a** (data not shown).

We next set out to examine whether perturbation of the structure and dynamics of duplex DNA induced by the noncovalent binding of an intercalator[68−70] or minor groove binding agent[71,72] would affect formation of the dA-AP ICL. We found that the classical intercalator ethidium bromide (EtBr),[68−70] at concentrations ≥0.5 μM, interferes with formation of the dA-AP ICL in duplex **1a** (Figure 6C). Unexpectedly, the lower yields of ICL were accompanied by the appearance of gel-shifted products migrating slightly slower than the AP-containing oligonucleotide, consistent with formation of an ethidium-AP aminoglycoside conjugate (Figure 6B). A nucleoside analog of the ethidium-AP adduct has been described previously,[73] but formation of such an adduct in duplex DNA is unprecedented. The formation of an ethidium-AP adduct proposed here is analogous to the reaction between 9-aminoellipticine and an AP site in duplex DNA reported previously.[74,75] Studies are underway to further characterize the formation and properties of this putative ethidium-AP adduct. Our results suggest that EtBr inhibits formation of the dA-AP ICL via covalent capture of the AP site. Thus, the question of whether the duplex distortion induced by the binding of an intercalator to duplex DNA[68] can inhibit formation of the dA-AP ICL remains unanswered for now.

Noncovalent association of the minor groove binding agent netropsin (Figure 7A) alters the structure of the double-helical DNA.[71,72,76] We designed two duplexes (**10** and **11**, Figure 7B) with A-rich, netropsin binding sites adjacent to, or overlapping, a dA-AP cross-linking sequence. We found that netropsin inhibits formation of the dA-AP ICL in these sequences. In contrast, netropsin did not inhibit ICL formation in duplex **9** that lacks an A-rich binding site for the ligand (Figure 7C).

The Base Excision Repair Glycosylase hAAG Decreases, but Does Not Completely Prevent, Formation of the dA-AP ICL. A previous report indicated that binding of the human monofunctional base excision repair glycosylase AAG (hAAG) to an AP-containing duplex prevented formation of an AP-derived ICL.[77] hAAG binds tightly to AP-containing duplexes but does not induce strand cleavage at the AP site.[78] The earlier studies examined the effects of hAAG on formation of an ICL derived from the reaction of 2-aminopurine[18,79] with an AP site.[77] Here we examined whether human hAAG inhibits formation of the dA-AP ICL in duplex **1a**. Consistent with the results of Admiraal and O'Brien,[77] we found that the presence of hAAG (1 equiv, 4 μM) inhibited formation of the dA-AP ICL in duplex **1a**. We observed a 1.8-fold decrease in ICL yield in the presence of hAAG (Figure S8); however, it is important to note that a significant amount of the dA-AP ICL (>20% yield) was still generated under these conditions. Incidentally, hAAG also inhibited spontaneous cleavage of the AP in the duplex **1a** (Figure S8).

The Presence of $NaBH_3CN$ Decreases the Yield of the dA-AP ICL. In our previous work, we characterized interstrand cross-links derived from the reaction of an AP site with a guanine residue on the opposing strand (Figure 1B).[13,15,82] In these reactions, inclusion of the water-compatible hydride reducing agent $NaBH_3CN$ (250 mM) leads to dramatically increased cross-link yields of a chemically stable alkylamine cross-link via a reductive amination reaction[15,82−84] An analogous reductive amination process that generates an alkylamine cross-link via reaction of an AP site with the noncanonical nucleobase 2-aminopurine also has been characterized.[18,79,85] On the other hand, it has not previously been determined whether the dA-AP ICL can similarly serve as a substrate for a reductive amination reaction.

Here, we found that incubation of the AP-containing duplex **2** in pH 5.2 sodium acetate buffer containing $NaBH_3CN$ (250 mM) *decreases* the ICL yield by a factor of 6 compared to the

https://doi.org/10.1021/acsomega.2c05736
ACS Omega 2022, 7, 36888−36901

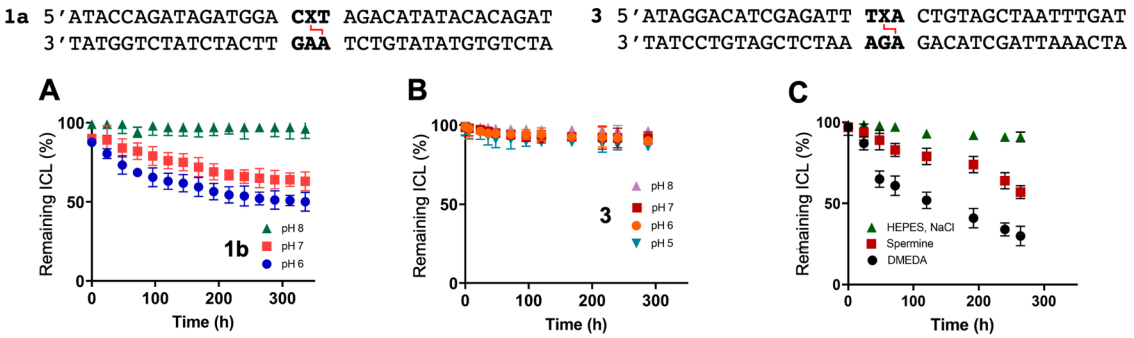

Figure 8. Stability of the dA-AP ICL in duplex DNA. (A) Stability of isolated dA-AP ICL in duplex **1a** at three different pH values. (B) Stability of isolated dA-AP ICL in duplex **3** at four different pH values. (C) Stability of the isolated dA-AP ICL in duplex **1a** in the presence of spermine (5 mM) or DMEDA (2 mM).

reaction in the absence of reducing agent (3 ± 1% versus 18 ± 3%, Figure S9). We are further investigating reductive amination in the context of the dA-AP ICL, but for the time being, we can only conclude that the behavior of dA-AP and dG-AP cross-links is quite different with respect to this reaction process.

Stability of the dA-AP ICL in Duplex DNA at Different pH Values and in the Presence of Polyamines. We isolated DNA duplexes **1a** and **3** containing the dA-AP ICL and studied the stability of the ICL under various conditions. The cross-linked duplexes were redissolved in sodium phosphate buffer at pH 6, 7, or 8 and the stability of the cross-link monitored by gel electrophoretic analysis. The cross-link in duplex **1a** was stable at pH 8 (Figure 8A). At pH values of 6 and 7, the ICL in **1a** dissociated slowly, with half-times in the range of 150 h (Figure 8A). In duplex **3**, dissociation of the ICL was largely independent of pH in the range 6−8, occurring with half-times of approximately 24 h (Figure 8B). In the presence of the polyamines, *N*,*N*′-dimethylethylenediamine (2 mM) or spermine (5 mM), the rate at which the ICL disappeared increased (Figure 8C), accompanied by generation of AP-derived cleavage products (Figure S10). Irreversible cleavage of the AP-containing duplex draws material away from the cross-link formation equilibria.

Duplexes Containing the dA-AP ICL Are Not Substrates for the DNA Repair Enzymes APE1 or Endo IV. AP sites in duplex DNA are cleaved by the repair enzymes apurinic/apyrimidinic endonuclease (APE1) in mammalian cells and by endonuclease IV (Endo IV) in bacterial cells.[86−88] Here we examined whether DNA duplexes containing the dA-AP ICL are substrates for APE1 or Endo IV. The cross-linked DNA duplexes were isolated and treated with APE1 or Endo IV. In the case of APE1, reactions were carried out in several different buffers optimized for AP endonuclease activity, exonuclease activity,[89] or nucleotide incision repair activity.[90] No cross-link unhooking or strand cleavage was observed for any of the duplexes containing the dA-AP ICL (Figure S11). Control reactions showed that the enzymes were active on uncross-linked AP sites in duplex DNA, as expected (Figure S11).

The dA-AP ICL Forms in Diverse Sequence Environments. Our previous work characterized formation of the dA-AP ICL in eight different sequences.[14,27,37,91] A recent study measured cross-link formation in an additional 13 sequences.[38] Here we used gel electrophoretic analysis to measure the yield of slowly migrating ICL bands generated in more than 40 different sequence contexts containing the core dA-AP cross-linking motif 5′-XN/5′AN (where N is any nucleobase and X = AP site). We varied the identity of the nucleobases neighboring and opposing the AP site (Figures 9 and S12). We also examined the ability of noncanonical nucleobases 2-aminopurine, 2,6-diaminopurine, N^6-methyladenosine, and an isoguanosine-isocytidine base pair to generate cross-links when substituted for adenine in the cross-linking motif.

We found that mispairing the cross-linked adenine residue in the dA-AP generates the highest ICL yields (FF−JJ, Figure 9). This is consistent with our previously published results with an A/A mispair.[37] Presumably, mispairing of the adenine residue involved in cross-link formation increases local duplex dynamics[92] and mitigates the energetic cost associated with separation of the A-T base pair normally required for ICL formation.[21] The high ICL yields observed in duplexes with mispaired adenine residues may be similar to the high cross-link yield generated near the end of duplex **6** (Figure 2) where dynamics are increased relative to the central regions of the duplex.[64] Placing the adenine residue into a bulge did not provide a high ICL yield (QQ, Figure 9). Pairing the cross-linked adenine residue against the universal base 5-nitroindole[93] gave a cross-link yield superior to the same 5′-AAC sequence with an A-T base pair at the cross-linking site (RR versus U, Figure 9). Mispairs on the 5′-side of the AP site disfavored ICL formation (DD, KK, LL, Figure 9).

Replacing the guanine residue with inosine in the core sequence **1a** did not significantly alter the ICL yield, suggesting that stacking of a three-purine run, and not reactivity of the exocyclic amino group in guanine, is responsible for the high yield in the 5′-AAG sequence (SS versus K, Figure 9). ICL yields were generally higher in sequences where a purine residue was located directly opposing the AP site, but significant ICL yields were nonetheless observed with pyrimidine resides in this position (V−AA, Figure 9). ICLs can form at AP sites located in the telomeric repeat sequence 5′GGGATT (BB, CC, Figure 9). Substitution of the cross-linking adenine residue with 2-aminopurine gave a relatively low ICL yield, while 2,6-diaminopurine gave approximately 20% ICL yield (A versus OO and TT, Figure 9). An isoguanosine-isocytidine base pair[94] at the cross-linking site gave a rather low ICL yield (A versus PP, Figure 9). Installation of an N^6-methyladenosine residue in the cross-linking position completely abrogated ICL formation (A versus UU, Figure 9). This result may be mechanistically interesting, perhaps suggesting that general acid−base-catalyzed elimination of water,[95] involving base-catalyzed removal of a proton from the N^6-amino group of adenine, is required to generate

https://doi.org/10.1021/acsomega.2c05736
ACS Omega 2022, 7, 36888−36901

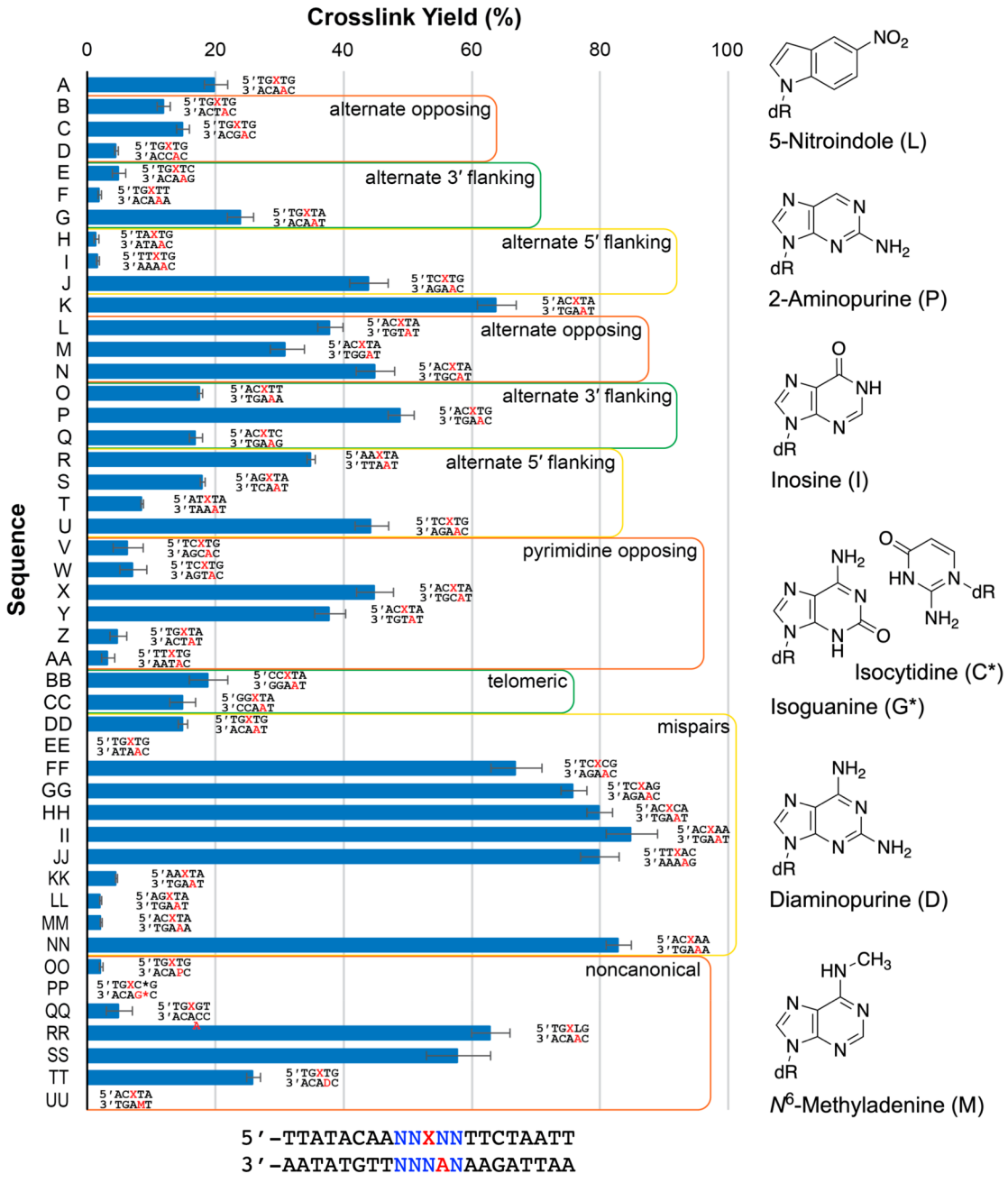

Figure 9. Effects of sequence variation on the yield of dA-AP ICL. The five-nucleotide cross-linking sequences shown above were contained in 35 nt duplexes, with the same flanking sequences shown at the bottom of the graph in the context of duplex **1a**. The designations "5′- and 3′-flanking" refer to the location with respect to the AP site. The structures of the noncanonical nucleobases examined here are shown on the right. Cross-linking reactions were carried out in HEPES buffer (50 mM, pH 7 or 7.4 containing 100 mM NaCl) for 120 h at 37 °C. The error bars reflect the standard deviation calculated from at least three measurements.

the dA-AP imine intermediate in the cross-linking reaction (the relevant proton is colored red in Figure 1A). The effect of N^6-methyladenine on ICL formation is interesting because this is an abundant noncanonical nucleobase in microorganisms.[96]

Other than the observations provided above, the effects of local sequence on the ICL yield generated in duplexes containing the dA-AP sequence motif are cryptic. Nonetheless, our findings, alongside earlier results[14,27,37,38,91] clearly demonstrate that the dA-AP ICL can form in a wide variety of sequence contexts. Indeed, the majority of the sequences examined here generated equilibrium ICL yields of 15% or more, and relatively few sequences produced ICL yields below 5%.

Formation of the dA-AP ICL in a DNA Hairpin. Hairpin-forming sequences can form short, stable duplexes (stem-loop structures).[97] Hairpin structures are important in biological systems[98,99] and in the design of functional nucleic acids.[100] Here we examined cross-link formation in a hairpin composed of an 11 nucleotide duplex containing a dA-AP ICL motif stabilized by a tetranucleotide loop (Figure 10A). We observed time-dependent formation of a new band generated upon incubation of the AP-containing hairpin **12** Figure 10B, lane 6). The half-maximal yield of ICL in this hairpin sequence

https://doi.org/10.1021/acsomega.2c05736
ACS Omega 2022, 7, 36888−36901

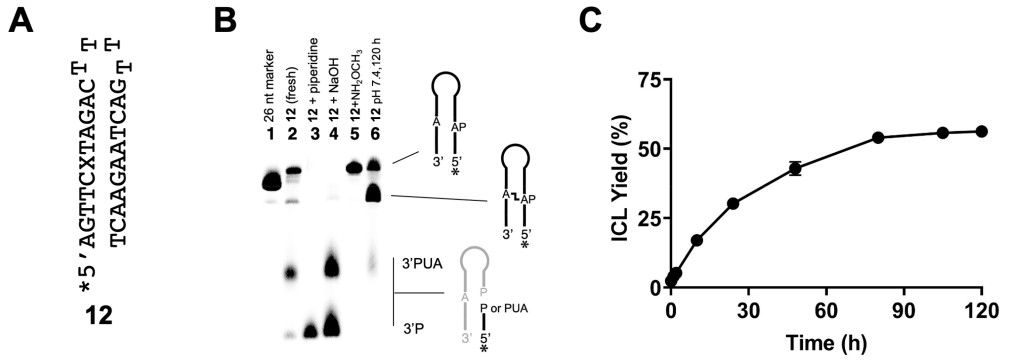

Figure 10. Formation of the dA-AP ICL in a DNA hairpin. (A) Hairpin sequence used in the experiment, X = AP site. (B) Gel electrophoretic analysis of hairpin formation. (C) Time course for the formation of dA-AP ICL in the hairpin sequence **12**.

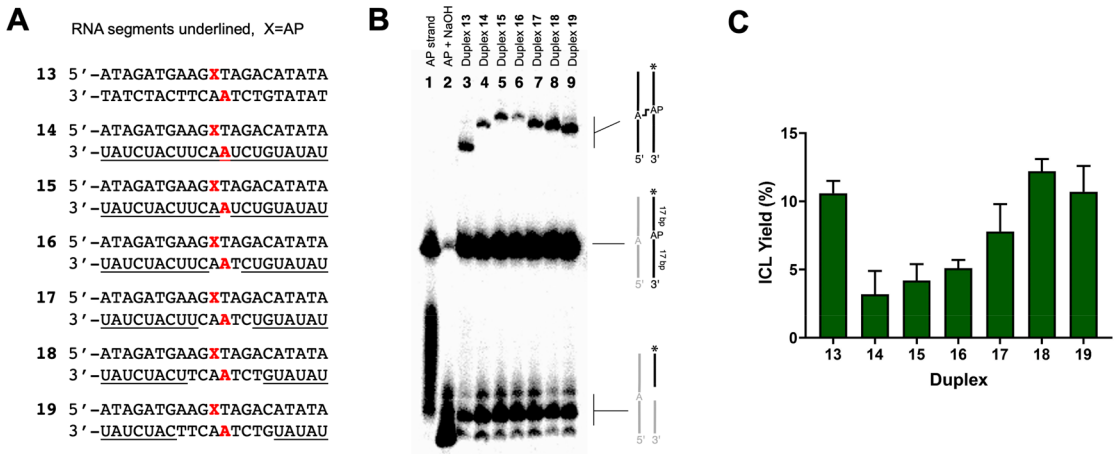

Figure 11. Formation of ICLs in DNA-RNA duplexes containing the dA-AP cross-linking motif. (A) Sequences used in the studies. (B) Gel electrophoretic analysis showing ICL formation (top band) and cleavage (bottom bands) of the AP-containing duplexes. The reactions were conducted in pH 7.4 HEPES buffer (50 mM containing 100 mM NaCl) at 37 °C for 120 h. Lane 1 shows the AP-containing strand from duplex **13** as a size marker. (C) Bar graph showing the yield of ICL from each duplex.

was reached by about 36 h and the final equilibrium yield (62 ± 3%) by about 90 h (Figure 10C).

Evidence that the new band was an AP-derived ICL was provided by an experiment showing that formation of this product was prevented by inclusion of the AP-trapping reagent methoxyamine (2 mM) in the reaction mixture (Figure 10B, lane 5). Further evidence that the new product arises from formation of a dA-AP ICL was provided by an experiment showing that an analogous sequence lacking the critical adenine residue in the cross-linking position failed to generate the new band (Figure S13). Interestingly, unlike the slow migration observed for DNA duplexes containing the dA-AP ICL, the cross-linked hairpin migrated *faster* in the denaturing polyacrylamide gel than the uncross-linked material, presumably because the compact nature of this species facilitates migration through the gel matrix.[101] A major signal observed in nanospray LC-ESI-TOF-MS analysis of the cross-linking reaction corresponded to a deconvoluted mass of 7823.27 Da, consistent with the calculated mass of the hairpin containing the dA-AP ICL (calcd 7823.31, Figure S14).

Formation of the dA-AP ICL in DNA-RNA Duplexes. Semlow et al. previously generated the dA-AP ICL in a DNA-RNA duplex, as part of a strategy to prepare a model substrate for the enzyme NEIL3.[26] In that earlier work, the AP site was located in an all-DNA oligomer that was paired with an opposing strand composed of all-RNA except for a three nucleotide 5′-TAA sequence of 2′-deoxyribonucleotides at the cross-linking site opposing the AP residue (the cross-linked adenine in this sequence is underlined). Here we examined ICL formation in a hybrid duplex with an all-RNA strand opposing an all-DNA AP-containing strand (Figure 11A). We further examined ICL formation in duplexes with varying numbers of DNA nucleotides flanking the adenine residue at the cross-linking site (duplexes **15**−**19**, Figure 11A).

We found that an ICL can be generated in the AP-containing DNA-RNA duplex **14**, though the yield was significantly lower than that produced by the analogous DNA−DNA duplex **13** (Figure 11B,C). Increasing the number of DNA nucleotides flanking the cross-linked adenine residue increased the ICL yield. Cross-linked duplexes with larger regions of DNA-RNA pairing migrated more slowly in the denaturing gel, perhaps indicating that there is less residual base pairing of the DNA-RNA regions in the denaturing gels. This supposition is consistent with our published data showing that "Y-shaped" cross-linked duplexes with unpaired, splayed arms on one side of the dA-AP cross-link migrate more slowly in a denaturing polyacrylamide gel than a fully base-paired duplex containing the cross-link.[27]

It is not surprising that different ICL yields were obtained in DNA-DNA and DNA-RNA duplexes. DNA-RNA duplexes are structurally distinct from typical B-form DNA-DNA double helices.[102,103] In addition, the junctions between DNA and

https://doi.org/10.1021/acsomega.2c05736
ACS Omega 2022, 7, 36888−36901

RNA segments in a hybrid duplex also present structural perturbations, with significant amounts of base pair buckle and propellor twist.[103] The ability of an all-DNA AP-containing oligomer to cross-link with an all-RNA strand (duplex **14**) suggests that AP-containing probes might be exploited for sequence-specific covalent capture of small cellular RNAs.[37] Our results also offer the possibility that AP-derived ICLs can form in the DNA-RNA hybrids generated during transcription of cellular DNA.[104,105]

CONCLUSIONS

AP sites are abundant lesions in cellular and synthetic DNA. ICLs derived from AP sites could be particularly important lesions because they block the replication and read-out of genetic information from double-stranded DNA.[26,106] Identification of a specialized eukaryotic repair pathway that unhooks the dA-AP ICL indicates potential biological relevance for this lesion.[26−28,107−109] The results presented here show that the dA-AP ICL forms under a wide range of reaction conditions and in a wide range of DNA sequences, thus providing further evidence that this cross-link could be widespread in both cellular and synthetic DNA.

EXPERIMENTAL SECTION

Materials. Oligonucleotides were purchased from Integrated DNA Technologies (IDT, Coralville, IA), Eurofins Genomics (Louisville, KY), and Sigma-Aldrich (St. Louis, MO). Some oligonucleotides purchased from IDT contained a 1,1′-diethyl-2,2′-dicarbocyanine (Cy5) fluorophore on the 5′-end and were HPLC purified before use. Uracil DNA glycosylase (UDG), human apurinic/apyrimidinic endonuclease (APE1), and endonuclease IV (Endo IV) were purchased from New England Biolabs (Ipswich, MA). [γ-^{32}P]-ATP (6000 C_i/mmol) was purchased from PerkinElmer, C-18 Sep-Pak cartridges were purchased from Waters (Milford, MA), BS Poly prep columns were obtained from BioRad (Hercules, CA), and acrylamide/bis-acrylamide 19:1 (40% solution, electrophoresis grade) was purchased from Fisher Scientific (Waltham, MA). Glutathione, $NaBH_3CN$, and buffers were purchased from Sigma-Aldrich (St. Louis, MO,). Quantification of radioactivity or fluorescence in polyacrylamide gels was carried out using a Personal Molecular Imager (BioRad) with Quantity One software (v.4.6.5). The pH of buffers was adjusted to the reported values at 24 °C. DMBAA (dimethylbutylammonium acetate) solutions used in the ESI-MS experiments was prepared as follows: a stock solution of *N*,*N*-dimethylbutylamine (7.125 M) was diluted to 100 mM with water and adjusted to pH 7.1 with glacial acetic acid.

Representative Cross-Linking Protocol. The single-stranded 2′-deoxyuridine (dU)-containing oligonucleotides were labeled on the 5′-end with either a ^{32}P-phosphoryl group or a 1,1′-diethyl-2,2′-dicarbocyanine (Cy5) fluorophore.[110,111] The single-stranded 2′-deoxyuridine (dU)-containing oligonucleotides were purified on a 20% polyacrylamide preparative gel prior to 5′-^{32}P-radiolabeling using standard methods.[110] The 5′-Cy5-labeled oligonucleotides were HPLC purified before use. The 5′-labeled dU-containing oligonucleotide were hybridized with the complementary oligonucleotide and treated with the enzyme uracil DNA glycosylase (UDG, final concentration of 200 units/mL) in Tris−HCl buffer (20 mM, pH 8) containing dithiothreitol (DTT, 1 mM) and EDTA (1 mM).[15,29−31] In some cases (e.g., experiments with DNA-RNA duplexes), single-stranded dU-containing oligodeoxynucleotide was treated with UDG to generate the AP-containing oligodeoxynucleotide which was hybridized with the appropriate complementary strand. After incubation at 37 °C for 2 h, the enzyme was removed by phenol−chloroform extraction and the DNA ethanol precipitated.[110] The resulting AP-containing oligonucleotide duplex was redissolved in the desired buffer and incubated at the appropriate temperature. In time-course experiments, aliquots were removed at prescribed times and stored frozen until gel electrophoretic analysis. For gel electrophoretic analysis, the reaction mixtures were combined with formamide loading buffer and loaded onto a 0.4 mm thick, 20% denaturing polyacrylamide gel (containing 7 M urea).[110] The gel images were obtained, and the amount of DNA in each band was quantitatively measured by fluorescence imaging or storage phosphor autoradiography.[32,111] For experiments characterizing properties of cross-linked DNA, the duplex containing the dA-AP ICL was isolated from a preparative 2 mm thick (preparative) 20% denaturing polyacrylamide gel. The slow-migrating band corresponding to the cross-linked DNA was excised from the gel with a razor blade. The gel slice was crushed, and the DNA was eluted into a buffer composed of EDTA (1 mM, pH 8) containing NaCl (200 mM) at room temperature for 1 h. The solution was filtered through a Poly-Prep column to remove the gel fragments, and the DNA ethanol was precipitated and stored at −80 °C prior to use.

Mass Spectrometric Analysis of the Cross-Linked Duplexes. LC−MS data were acquired on an Agilent Technologies 6520A Accurate Mass QTOF. Samples were analyzed according to the protocol of Studzińska and Buszewski,[112] with slight modifications as outlined. The sample was injected onto a C8 trap column (Michrom Bioresources Captrap) at a flow rate of 5 μL/min of 10 mM DMBAA, pH 7.1 over 4 min, and separated by isocratic elution (either 80% or 42.5% methanol, 15 mM DMBAA, pH 7.1) at a flow rate of 0.4 μL/min on a 10 cm × 75 μm C8 analytical column (fused silica packed with Michrom Bioresources C8, 3.5 μm particles). Following the 4 min trap load, separation on the trap/analytical columns continued for 16 min under isocratic elution conditions. The total run time was 20 min. Mass spectra were acquired using the following parameters: negative-ion mode; VCap 2500 V; mass range 290−3200 m/z; 0.63 spectra/second; fragmentor at 300 V (250 V for IDT oligo); internal MS recalibration was achieved using the K/Na adducted Hexakis 1221 Chip Cube High Mass Reference compound (m/z 1279.99). Samples were loaded in sequence as follows: blank (10 mM DMBAA), sample, and blank. Multiply charged DNA peaks were deconvoluted using the maximum entropy algorithm in Qualitative Analysis software (version B.07.00 Agilent Technologies) with the following parameters: adduct = proton-loss; m/z range = 600−1500 m/z; mass range = expected mass ±2 kDa; peak height to calculate mass = 25%. The m/z values reported are neutral deconvoluted masses. The cross-linking reactions were carried out as described above. After 72 h of incubation, 20 vol of ammonium acetate (2.5 M) was added. After 30 min at room temperature, the mixture was desalted using a C18 Sep-Pak column eluted with HPLC-grade methanol and ultrapure, deionized water.

https://doi.org/10.1021/acsomega.2c05736
ACS Omega 2022, 7, 36888−36901

■ ASSOCIATED CONTENT

Supporting Information

The Supporting Information is available free of charge at https://pubs.acs.org/doi/10.1021/acsomega.2c05736.

Additional information on formation of the dA-AP ICL including pH effects, buffer effects, effects of neighboring sequence, effects of various additives, and formation in a DNA hairpin (PDF)

■ AUTHOR INFORMATION

Corresponding Author

Kent S. Gates − *Department of Biochemistry, University of Missouri, Columbia, Missouri 65211, United States; Department of Chemistry, University of Missouri, Columbia, Missouri 65211, United States;* orcid.org/0000-0002-4218-7411; Email: gatesk@missouri.edu

Authors

Saosan Binth Md. Amin − *Department of Chemistry, University of Missouri, Columbia, Missouri 65211, United States*

Tanhaul Islam − *Department of Chemistry, University of Missouri, Columbia, Missouri 65211, United States*

Nathan E. Price − *Department of Chemistry, University of Missouri, Columbia, Missouri 65211, United States*

Amanda Wallace − *Department of Chemistry, University of Missouri, Columbia, Missouri 65211, United States*

Xu Guo − *Department of Chemistry, University of Missouri, Columbia, Missouri 65211, United States*

Anuoluwapo Gomina − *Department of Chemistry, University of Missouri, Columbia, Missouri 65211, United States;* orcid.org/0000-0002-2874-3119

Marjan Heidari − *Department of Chemistry, University of Missouri, Columbia, Missouri 65211, United States*

Kevin M. Johnson − *Department of Chemistry, University of Missouri, Columbia, Missouri 65211, United States*

Calvin D. Lewis − *Department of Chemistry, University of Missouri, Columbia, Missouri 65211, United States*

Zhiyu Yang − *Department of Chemistry, University of Missouri, Columbia, Missouri 65211, United States;* Present Address: Department of Bioengineering, Massachusetts Institute of Technology, Bld. 56-669, 77 Massachusetts Ave, Cambridge, MA 02139-4307

Complete contact information is available at: https://pubs.acs.org/10.1021/acsomega.2c05736

Notes

The authors declare no competing financial interest.

■ ACKNOWLEDGMENTS

We are grateful to the National Science Foundation (NSF-CHE 1808672) and the National Institutes of Health (ES021007 to K.S.G.) for financial support of this work.

■ REFERENCES

(1) Lindahl, T.; Karlstrom, O. Heat-induced depyrimidination of deoxyribonucleic acid in solution. *Biochemistry* **1973**, *12*, 5151−5154.

(2) Lindahl, T.; Nyberg, B. Rate of depurination of native deoxyribonucleic acid. *Biochemistry* **1972**, *11* (19), 3610−3618.

(3) Gates, K. S.; Nooner, T.; Dutta, S. Biologically relevant chemical reactions of N7-alkyl-2'-deoxyguanosine adducts in DNA. *Chem. Res. Toxicol.* **2004**, *17* (7), 839−856.

(4) Krokan, H. E.; Bjørås, M. Base Excision Repair. *Cold Spring Harb. Perspect. Biol.* **2013**, *5* (4), a012583.

(5) Stivers, J. T.; Jiang, Y. J. A mechanistic perspective on the chemistry of DNA repair glycosylases. *Chem. Rev.* **2003**, *103*, 2729−2759.

(6) Chen, H.; Yao, L.; Brown, C.; Rizzo, C. J.; Turesky, R. J. Quantitation of Apurinic/Apyrimidinic Sites in Isolated DNA and in Mammalian Tissue with a Reduced Level of Artifacts. *Anal. Chem.* **2019**, *91* (11), 7403−7410.

(7) Guo, J.; Chen, H.; Upadhyaya, P.; Zhao, Y.; Turesky, R. J.; Hecht, S. S. Mass Spectrometric Quantitation of Apurinic/Apyrimidinic Sites in Tissue DNA of Rats Exposed to Tobacco-Specific Nitrosamines and in Lung and Leukocyte DNA of Cigarette Smokers and Nonsmokers. *Chem. Res. Toxicol.* **2020**, *33* (9), 2475−2486.

(8) Wilde, J. A.; Bolton, P. H.; Mazumdar, A.; Manoharan, M.; Gerlt, J. A. Characterization of the equilibrating forms of the abasic site in duplex DNA using 17O-NMR. *J. Am. Chem. Soc.* **1989**, *111*, 1894−1896.

(9) Freese, E.; Cashel, M. Crosslinking of deoxyribonucleic acid by exposure to low pH. *Biochim. Biophys. Acta* **1964**, *91*, 67−77.

(10) Burnotte, J.; Verly, W. G. Crosslinking of methylated DNA by moderate heating at neutral pH. *Biochim. Biophys. Acta* **1972**, *262*, 449−452.

(11) Goffin, C.; Verly, W. G. Interstrand crosslinks due to AP (apurinic/apyrimidinic) sites. *FEBS Lett.* **1983**, *161* (1), 140−144.

(12) Goffin, C.; Verly, W. G. Some properties of the interstrand crosslinks in depurinated DNA. *Biochim. Biophys. Acta* **1984**, *783*, 1−5.

(13) Dutta, S.; Chowdhury, G.; Gates, K. S. Interstrand crosslinks generated by abasic sites in duplex DNA. *J. Am. Chem. Soc.* **2007**, *129*, 1852−1853.

(14) Price, N. E.; Johnson, K. M.; Wang, J.; Fekry, M. I.; Wang, Y.; Gates, K. S. Interstrand DNA-DNA Cross-Link Formation Between Adenine Residues and Abasic Sites in Duplex DNA. *J. Am. Chem. Soc.* **2014**, *136*, 3483−3490.

(15) Johnson, K. M.; Price, N. E.; Wang, J.; Fekry, M. I.; Dutta, S.; Seiner, D. R.; Wang, Y.; Gates, K. S. On the Formation and Properties of Interstrand DNA-DNA Cross-links Forged by Reaction of an Abasic Site With the Opposing Guanine Residue of 5′-CAp Sequences in Duplex DNA. *J. Am. Chem. Soc.* **2013**, *135*, 1015−1025.

(16) Varela, J. G.; Pierce, L. E.; Guo, X.; Price, N. E.; Johnson, K. M.; Yang, Z.; Wang, Y.; Gates, K. S. Interstrand Cross-Link Formation Involving Reaction of a Mispaired Cytosine Residue with an Abasic Site in Duplex DNA. *Chem. Res. Toxicol.* **2021**, *34*, 1124−1132.

(17) Gamboa Varela, J.; Gates, K. S. A Simple, High-Yield Synthesis of DNA Duplexes Containing a Covalent, Thermally-Reversible Interstrand Cross-link At a Defined Location. *Angew. Chem., Int. Ed. Engl.* **2015**, *54*, 7666−7669.

(18) Imani-Nejad, M.; Price, N. E.; Haldar, T.; Lewis, C.; Wang, Y.; Gates, K. S. Interstrand DNA cross-links derived from reaction of a 2-aminopurine residue with an abasic site. *ACS Chem. Biol.* **2019**, *14*, 1481−1489.

(19) Yang, Z.; Price, N. E.; Johnson, K. M.; Wang, Y.; Gates, K. S. Interstrand cross-links arising from strand breaks at true abasic sites in duplex DNA. *Nucleic Acids Res.* **2017**, *45*, 6275−6283.

(20) Housh, K.; Jha, J. S.; Yang, Z.; Haldar, T.; Johnson, K. M.; Yin, J.; Wang, Y.; Gates, K. S. Formation and Repair of an Interstrand DNA Cross-Link Arising from a Common Endogenous Lesion. *J. Am. Chem. Soc.* **2021**, *143*, 15344−15357.

(21) Kellum, A. H.; Qiu, D. Y.; Voehler, M. W.; Martin, W.; Gates, K. S.; Stone, M. P. Structure of a Stable Interstrand DNA Cross-Link Involving a *β*-N-Glycosyl Linkage Between an N6-dA Amino Group and an Abasic Site. *Biochemistry* **2020**, DOI: 10.1021/acs.biochem.0c00596.

(22) Price, N. E.; Catalano, M. J.; Liu, S.; Wang, Y.; Gates, K. S. Chemical and structural characterization of interstrand cross-links formed between abasic sites and adenine residue in duplex DNA. *Nucleic Acids Res.* **2015**, *43*, 3434−3441.

(23) Catalano, M. J.; Liu, S.; Andersen, N.; Yang, Z.; Johnson, K. M.; Price, N. A.; Wang, Y.; Gates, K. S. Chemical structure and properties of the interstrand cross-link formed by the reaction of guanine residues with abasic sites in duplex DNA. *J. Am. Chem. Soc.* **2015**, *137*, 3933−3945.
(24) Hopkins, P. B.; Millard, J. T.; Woo, J.; Weidner, M. F.; Kirchner, J. J.; Sigurdsson, S. T.; Raucher, S. Sequence preferences of DNA interstrand cross-linking agents: Importance of minimal DNA structural reorganization in the cross-linking reactions of mechlorethamine, cisplatin, and mitomycin C. *Tetrahedron* **1991**, *47* (14/15), 2475−2489.
(25) Semlow, D. R.; MacKrell, V. A.; Walter, J. C. The HMCES DNA-protein cross-link functions as an intermediate in DNA interstrand cross-link repair. *Nat. Struct Mol. Biol.* **2022**, *29* (5), 451−462.
(26) Semlow, D. R.; Zhang, J.; Budzowska, M.; Drohat, A. C.; Walter, J. C. Replication-dependent unhooking of DNA interstrand cross-links by the NEIL3 glycosylase. *Cell* **2016**, *167*, 498−511.
(27) Imani-Nejad, M.; Housh, K.; Rodriguez, A. A.; Haldar, T.; Kathe, S.; Wallace, S. S.; Eichman, B. F.; Gates, K. S. Unhooking of an interstrand cross-link at DNA fork structures by the DNA glycosylase NEIL3. *DNA Repair* **2020**, *86*, 102752.
(28) Yang, Z.; Nejad, M. I.; Gamboa Varela, J.; Price, N. E.; Wang, Y.; Gates, K. S. A role for the base excision repair enzyme NEIL3 in replication-dependent repair of interstrand cross-links derived from psoralen and abasic sites. *DNA Repair* **2017**, *52*, 1−11.
(29) Lindahl, T.; Ljunquist, S.; Siegert, W.; Nyberg, B.; Sperens, B. DNA N-glycosidases: properties of uracil-DNA glycosidase from Escherichia coli. *J. Biol. Chem.* **1977**, *252*, 3286−3294.
(30) Varshney, U.; van de Sande, J. H. Specificities and kinetics of uracil excision from uracil-containing DNA oligomers by Escherichia coli uracil DNA glycosylase. *Biochemistry* **1991**, *30*, 4055−4061.
(31) Stuart, G. R.; Chambers, R. W. Synthesis and properties of oligodeoxynucleotides with an AP site at a preselected position. *Nucleic Acids Res.* **1987**, *15* (18), 7451−7462.
(32) Johnston, R. F.; Pickett, S. C.; Barker, D. L. Autoradiography using storage phosphor technology. *Electrophoresis* **1990**, *11* (5), 355−360.
(33) Gates, K. S. An overview of chemical processes that damage cellular DNA: spontaneous hydrolysis, alkylation, and reactions with radicals. *Chem. Res. Toxicol.* **2009**, *22* (11), 1747−1760.
(34) Haldar, T.; Jha, J. S.; Yang, Z.; Nel, C.; Housh, K.; Cassidy, O. J.; Gates, K. S. Unexpected Complexity in the Products Arising from NaOH-, Heat-, Amine-, and Glycosylase-Induced Strand Cleavage at an Abasic Site in DNA. *Chem. Res. Toxicol.* **2022**, *35* (2), 218−232.
(35) Jha, J. S.; Nel, C.; Haldar, T.; Peters, D.; Housh, K.; Gates, K. S. Products generated by amine-catalyzed strand cleavage at apurinic/apyrimidinic sites in DNA: new insights from a biomimetic nucleoside model system. *Chem. Res. Toxicol.* **2022**, *35*, 203−217.
(36) Catalano, M. J.; Price, N. E.; Gates, K. S. Effective molarity in a nucleic acid controlled reaction. *Bioorg. Med. Chem. Lett.* **2016**, *26* (11), 2627−2630.
(37) Nejad, M. I.; Shi, R.; Zhang, X.; Gu, L.-Q.; Gates, K. S. Sequence-specific covalent capture coupled with high-contrast nanopore detection of a disease-derived nucleic acid sequence. *ChemBioChem.* **2017**, *18*, 1383−1386.
(38) Huskova, A.; Landova, B.; Boura, E.; Silhan, J. The rate of formation and stability of abasic site interstrand crosslinks in the DNA duplex. *DNA Repair (Amst)* **2022**, *113*, 103300.
(39) McIlvaine, T. C. A buffer solution for colorimetric comparison. *J. Biol. Chem.* **1921**, *49*, 183−186.
(40) Cordes, E. H.; Jencks, W. P. On the mechanism of Schiff base formation and hydrolysis. *J. Am. Chem. Soc.* **1962**, *84*, 832−837.
(41) Casey, J. R.; Grinstein, S.; Orlowski, J. Sensors and regulators of intracellular pH. *Nat. Rev. Mol. Cell Biol.* **2010**, *11* (1), 50−61.
(42) Trindade, D. F.; Cerchiaro, G.; Augusto, O. A role for peroxymonocarbonate in the stimulation of biothiol peroxidation by the bicarbonate/carbon dioxide pair. *Chem. Res. Toxicol.* **2006**, *19*, 1475−1482.
(43) Mannisto, J. K.; Pavlovic, L.; Tiainen, T.; Nieger, M.; Sahari, A.; Hopmann, K. H.; Repo, T. Mechanistic insights into carbamate formation from CO2 and amines: the role of guanidine-CO2 adducts. *Catal. Sci. Technol.* **2021**, *11*, 6877−6886.
(44) Linthwaite, V. L.; Janus, J. M.; Brown, A. P.; Wong-Pascua, D.; O'Donoghue, A. C.; Porter, A.; Treumann, A.; Hodgson, D. R. W.; Cann, M. J. The identification of carbon dioxide mediated protein post-translational modifications. *Nat. Commun.* **2018**, *9* (1), 3092.
(45) Niedernhofer, L. J.; Riley, M.; Schnetz-Boutaud, N.; Sanduwaran, G.; Chaudhary, A. K.; Reddy, G. R.; Marnett, L. J. Temperature-dependent formation of a conjugate between tris-(hydroxymethyl)aminomethane buffer and the malondialdehyde-DNA adduct pyrimidopurinone. *Chem. Res. Toxicol.* **1997**, *10* (5), 556−61.
(46) Gallopo, A. R.; Cleland, W. W. Properties of 3-hydroxypropionaldehyde 3-phosphate. *Arch. Biochem. Biophys.* **1979**, *195* (1), 152−154.
(47) Burcham, P. C.; Fontaine, F. R.; Petersen, D. R.; Pyke, S. M. Reactivity with Tris(hydroxymethyl)aminomethane confounds immunodetection of acrolein-adducted proteins. *Chem. Res. Toxicol.* **2003**, *16* (10), 1196−201.
(48) Mazumder, A.; Gerlt, J. A.; Absalon, M. J.; Stubbe, J.; Cunningham, R. P.; Withka, J.; Bolton, P. H. Stereochemical studies of the b-elimination reactions at aldehydic abasic sites in DNA: endonuclease III from Escherichia coli, sodium hydroxide, and Lys-Trp-Lys. *Biochemistry* **1991**, *30* (4), 1119−26.
(49) Kushida, T.; Uesugi, M.; Sugiura, Y.; Kigoshi, H.; Tanaka, H.; Hirokawa, J.; Ojika, M.; Yamada, K. DNA damage by ptaquiloside, a potent bracken carcinogen: detection of selective strand breaks and identification of DNA-cleavage products. *J. Am. Chem. Soc.* **1994**, *116*, 479−486.
(50) Every, A. E.; Russu, I. M. Influence of magnesium ions on spontaneous opening of DNA base pairs. *J. Phys. Chem. B* **2008**, *112* (25), 7689−95.
(51) Chakraborti, A. K.; Bhagat, S.; Rudrawar, S. Magnesium perchlorate as an efficient catalyst for the synthesis of imines and phenylhydrazones. *Tetrahedron Lett.* **2004**, *45*, 7641−7644.
(52) Meister, A. Glutathione metabolism and its selective modification. *J. Biol. Chem.* **1988**, *263*, 17205−1720.
(53) Soboll, S.; Grundel, S.; Harris, J.; Kolb-Bachofen, V.; Ketterer, B.; Sies, H. The content of glutathione and glutathione S-transferases and the glutathione peroxidase activity in rat liver nuclei determined by a non-aqueous technique of cell fractionation. *Biochem. J.* **1995**, *311*, 889−894.
(54) Lienhard, G. E.; Jencks, W. P. Thiol Addition to the Carbonyl Group. Equilibria and Kinetics. *J. Am. Chem. Soc.* **1966**, *88*, 3982−3995.
(55) Kallen, R. G.; Jencks, W. P. The mechanism of the condensation of formaldehyde with tetrahydrofolic acid. *J. Biol. Chem.* **1966**, *241* (24), 5851−5863.
(56) Ghodke, P. P.; Matse, J. H.; Dawson, S.; Guengerich, F. P. Nucleophilic Thiol Proteins Bind Covalently to Abasic Sites in DNA. *Chem. Res. Toxicol.* **2022**, DOI: 10.1021/acs.chemrestox.2c00068.
(57) Cordes, E. H.; Jencks, W. P. Nucleophilic Catalysis of Semicarbazone Formation by Anilines. *J. Am. Chem. Soc.* **1962**, *84*, 826−831.
(58) Dirksen, A.; Dirksen, S.; Hackeng, T. M.; Dawson, P. E. Nucleophilic Catalysis of Hydrazone Formation and Transimination: Implications for Dynamic Covalent Chemistry. *J. Am. Chem. Soc.* **2006**, *128*, 15602−15603.
(59) Larsen, D.; Pittelkow, M.; Karmakar, S.; Kool, E. T. New organocatalyst scaffolds with high activity in promoting hydrazone and oxime at neutral pH. *Org. Lett.* **2015**, *17*, 274−277.
(60) Ollivier, N.; Agouridas, V.; Snella, B.; Desmet, R.; Drobecq, H.; Vicogne, J.; Melnyk, O. Catalysis of Hydrazone and Oxime Peptide Ligation by Arginine. *Org. Lett.* **2020**, *22* (21), 8608−8612.
(61) Larsen, D.; Kietrys, A. M.; Clark, S. A.; Park, H. S.; Ekebergh, A.; Kool, E. T. Exceptionally Rapid Oxime and Hydrazone Formation

https://doi.org/10.1021/acsomega.2c05736
ACS Omega 2022, 7, 36888−36901

Promoted by Catalytic Amine Buffers with Low Toxicity. *Chem. Sci.* **2018**, *9*, 5252−5259.
(62) Song, Z.-W.; Li, M.-H.; Cheng, C.-M.; Chen, L.-Q.; Guo, X.-Q.; Wang, R.-J.; Wu, G.-S.; Zhao, Y.-F. Structure study on N-phenyl-2-deoxy-D-ribopyranosylamine. *Chin. J. Struct. Chem.* **2007**, *26*, 1476−1480.
(63) McHugh, P. J.; Knowland, J. Novel reagents for chemical cleavage at abasic sites and UV photoproducts in DNA. *Nucleic Acids Res.* **1995**, *23* (10), 1664−1670.
(64) Andreatta, D.; Sen, S.; Perez Lustres, J. L.; Kovalenko, S. A.; Ernsting, N. P.; Murphy, C. J.; Coleman, R. S.; Berg, M. A. Ultrafast dynamics in DNA: "fraying" at the end of the helix. *J. Am. Chem. Soc.* **2006**, *128* (21), 6885−92.
(65) Rosa, S.; Fortini, P.; Karran, P.; Bignami, M.; Dogliotti, E. Processing in vitro of an abasic site reacted with methoxyamine: a new assay for the detection of abasic sites formed in vivo. *Nucleic Acids Res.* **1991**, *19* (20), 5569−5574.
(66) Liuzzi, M.; Talpaert-Borle, M. A new approach to the study of the base-excision repair pathway using methoxyamine. *J. Biol. Chem.* **1985**, *260* (9), 5252−8.
(67) Melton, D.; Lewis, C. D.; Price, N. E.; Gates, K. S. Covalent adduct formation between the antihypertensive drug hydralazine and abasic sites in double- and single-stranded DNA. *Chem. Res. Toxicol.* **2014**, *27*, 2113−2118.
(68) Galindo-Murillo, R.; Cheatham, T. E. Ethidium bromide interactions with DNA: an exploration of a classic DNA-ligand complex with unbiased molecular dynamics simulations. *Nucleic Acids Res.* **2021**, *49* (7), 3735−3747.
(69) LePecq, J. B.; Paoletti, C. A fluorescent complex between ethidium bromide and nucleic acids. Physical-chemical characterization. *J. Mol. Biol.* **1967**, *27* (1), 87−106.
(70) Waring, M. J. Complex formation between ethidium bromide and nucleic acids. *J. Mol. Biol.* **1965**, *13* (1), 269−82.
(71) Storl, K.; Burckhardt, G.; Lown, J. W.; Zimmer, C. Studies on the ability of minor groove binders to induce supercoiling in DNA. *FEBS Lett.* **1993**, *334* (1), 49−54.
(72) Coll, M.; Aymami, J.; van der Marel, G. A.; van Boom, J. H.; Rich, A.; Wang, A. H. Molecular structure of the netropsin-d(CGCGATATCGCG) complex: DNA conformation in an alternating AT segment. *Biochemistry* **1989**, *28* (1), 310−20.
(73) Amann, N.; Wagenknecht, H.-A. Synthesis of an ethidium nucleoside and its acyclic analog. *Tetrahedron Lett.* **2003**, *44*, 1685−1690.
(74) Bertrand, J.-R.; Vasseur, J.-J.; Gouyette, A.; Rayner, B.; Imbac, J.-L.; Paoletti, C.; Malvy, C. Mechanism of Cleavage of Apurinic Sites by 9-Aminoellipticin. *J. Biol. Chem.* **1989**, *264*, 14172−14178.
(75) Singh, M. P.; Hill, G. C.; Péoc'h, D.; Rayner, B.; Imbach, J.-L.; Lown, J. W. High-field NMR and restrained molecular modeling studies on a DNA heteroduplex containing a modified apurinic abasic site in the form of a covalently linked 9-aminoellipticine. *Biochemistry* **1994**, *33*, 10271−10285.
(76) Chen, Y. Z.; Prohofsky, E. W. Calculation of the dynamics of drug binding in a netropsin-DNA complex. *Phys. Rev. E* **1995**, *51*, 5048.
(77) Admiraal, S. J.; O'Brien, P. J. Base Excision Repair Enzymes Protect Abasic Sites in Duplex DNA from Interstrand Cross-Links. *Biochemistry* **2015**, *54* (9), 1849−1857.
(78) Abner, C. W.; Lau, A. Y.; Ellenberger, T.; Bloom, L. B. Base excision and DNA binding activities of human alkyladenine DNA glycosylase are sensitive to the base paired with a lesion. *J. Biol. Chem.* **2001**, *276* (16), 13379−87.
(79) Tang, J.; Tang, F.; Zhao, L. Facile preparation of model DNA interstrand cross-link repair intermediates using ribonucleotide-containing DNA. *DNA Repair (Amst)* **2022**, *111*, 103286.
(80) Tse, W. C.; Boger, D. L. A fluorescent intercalator displacement assay for establishing DNA binding selectivity and affinity. *Acc. Chem. Res.* **2004**, *37*, 61−69.
(81) Ward, B.; Rehfuss, R.; Goodisman, J.; Dabrowiak, J. C. Determination of netropsin-DNA binding constants from footprinting data. *Biochemistry* **1988**, *27* (4), 1198−205.
(82) Nejad, M. I.; Guo, X.; Housh, K.; Nel, C.; Yang, Z.; Price, N. E.; Wang, Y.; Gates, K. S. Preparation and purification of oligodeoxynucleotide duplexes containing a site-specific, reduced, chemically stable covalent interstrand cross-link between a guanine residue and an abasic site. *Methods Mol. Biol.* **2019**, *1973*, 163−175.
(83) Borch, R. F.; Bernstein, M. D.; Durst, H. D. The cyanohydridoborate anion as a selective reducing agent. *J. Am. Chem. Soc.* **1971**, *93* (12), 2897−2904.
(84) Borch, R. F.; Hassid, A. I. A new method for the methylation of amines. *J. Org. Chem.* **1972**, *37*, 1673−1674.
(85) Tang, J.; Zhao, L. Preparation of DNA interstrand cross-link repair intermediates induced by abasic sites. *MethodsX* **2022**, *9*, 101687.
(86) Daley, J. M.; Zakaria, C.; Ramotar, D. The endonuclease IV family of apurinic/apyrimidinic endonucleases. *Mutat. Res.* **2010**, *705* (3), 217−27.
(87) Hosfield, D. J.; Guan, Y.; Haas, B. J.; Cunningham, R. P.; Tainer, J. A. Structure of the DNA repair enzyme endonuclease IV and its DNA complex: double-nucleotide flipping at abasic sites and three-metal-ion catalysis. *Cell* **1999**, *98* (3), 397−408.
(88) Whitaker, A. M.; Freudenthal, B. D. APE1: A skilled nucleic acid surgeon. *DNA Repair* **2018**, *71*, 93−100.
(89) Chou, K.-m.; Cheng, Y.-c. The exonuclease activity of human apurinic/apyrimidinic endonuclease (APE1). *J. Biol. Chem.* **2003**, *278* (20), 18289−18296.
(90) Gros, L.; Ishchenko, A. A.; Ide, H.; Elder, R. H.; Saparbaev, M. K. The major human AP endonuclease (Ape1) is involved in the nucleotide incision repair pathway. *Nucleic Acids Res.* **2004**, *32* (1), 73−81.
(91) Nejad, M. I.; Johnson, K. M.; Price, N. E.; Gates, K. S. A new cross-link for an old cross-linking drug: the nitrogen mustard anticancer agent mechlorethamine generates cross-links derived from abasic sites in addition to the expected drug-bridged cross-links. *Biochemistry* **2016**, *55* (16), 7033−7041.
(92) Rossetti, G.; Dans, P. D.; Gomez-Pinto, I.; Ivani, I.; Gonzalez, C.; Orozco, M. The structural impact of DNA mismatches. *Nucleic Acids Res.* **2015**, *43* (8), 4309−4321.
(93) Loakes, D.; Brown, D. M. 5-Nitroindole as an universal base analogue. *Nucleic Acids Res.* **1994**, *22* (20), 4039−43.
(94) Roberts, C.; Bandaru, R.; Switzer, C. Theoretical and Experimental Study of Isoguanine and Isocytosine: Base Pairing in an Expanded Genetic System. *J. Am. Chem. Soc.* **1997**, *119* (20), 4640−4649.
(95) Sayer, J. M.; Peskin, M.; Jencks, W. P. Imine-forming elimination reactions. I. General base and acid catalysis and influence of the nitrogen substituent on rates and equilibria for carbinolamine dehydration. *J. Am. Chem. Soc.* **1973**, *95* (13), 4277.
(96) Wion, D.; Casadesus, J. N6-methyl-adenine: an epigenetic signal for DNA-protein interactions. *Nat. Rev. Microbiol* **2006**, *4* (3), 183−92.
(97) Senior, M. M.; Jones, R. A.; Breslauer, K. J. Influence of loop residues on the relative stabilities of DNA hairpin structures. *Proc. Natl. Acad. Sci. U.S.A.* **1988**, *85*, 6242−6246.
(98) Nadel, Y.; Weisman-Shomer, P.; Fry, M. The fragile X syndrome single strand d(CGG)n nucleotide repeats readily fold back to form unimolecular hairpin structures. *J. Biol. Chem.* **1995**, *270* (48), 28970−7.
(99) Xu, M.; Gabison, J.; Liu, Y. Trinucleotide repeat deletion via a unique hairpin bypass by DNA polymerase beta and alternate flap cleavage by flap endonuclease 1. *Nucleic Acids Res.* **2013**, *41* (3), 1684−97.
(100) Vieregg, J. R.; Nelson, H. M.; Stoltz, B. M.; Pierce, N. A. Selective nucleic acid capture with shielded covalent probes. *J. Am. Chem. Soc.* **2013**, *135* (26), 9691−9699.

https://doi.org/10.1021/acsomega.2c05736
ACS Omega 2022, 7, 36888−36901

(101) Ashley, G. W.; Kushlan, D. M. Chemical synthesis of oligodeoxynucleotide dumbbells. *Biochemistry* **1991**, *30* (11), 2927−33.
(102) Davis, R. R.; Shaban, N. M.; Perrino, F. W.; Hollis, T. Crystal structure of RNA-DNA duplex provides insight into conformational changes induced by RNase H binding. *Cell Cycle* **2015**, *14* (4), 668−73.
(103) Hsu, S. T.; Chou, M. T.; Cheng, J. W. The solution structure of [d(CGC)r(aaa)d(TTTGCG)](2): hybrid junctions flanked by DNA duplexes. *Nucleic Acids Res.* **2000**, *28* (6), 1322−31.
(104) Crossley, M. P.; Bocek, M.; Cimprich, K. A. R-Loops as Cellular Regulators and Genomic Threats. *Mol. Cell* **2019**, *73* (3), 398−411.
(105) Tang, S.; Stokasimov, E.; Cui, Y.; Pellman, D. Breakage of cytoplasmic chromosomes by pathological DNA base excision repair. *Nature* **2022**, *606* (7916), 930−936.
(106) Yang, Z.; Johnson, K. M.; Price, N. E.; Gates, K. S. Characterization of interstrand DNA-DNA cross-links derived from abasic sites using bacteriophage φ29 DNA polymerase. *Biochemistry* **2015**, *54*, 4259−4266.
(107) Semlow, D. R.; MacKrell, V. A.; Walter, J. C. The HMCES DNA-protein cross-link functions as a constitutive DNA repair intermediate. *Nat. Struct. Mol. Biol.* **2022**, *29*, 451−462.
(108) Rodriguez, A. A.; Wojtaszek, J. L.; Greer, B. H.; Haldar, T.; Gates, K. S.; Williams, R. S.; Eichman, B. F. An autoinhibitory role for the GRF zinc finger domain of DNA glycosylase NEIL3. *J. Biol. Chem.* **2020**, *295*, 15566.
(109) Li, N.; Wang, J.; Wallace, S. S.; Chen, J.; Zhou, J.; D'Andrea, A. D. Cooperation of the NEIL3 and Fanconi anemia/BRCA pathways in interstrand crosslink repair. *Nucleic Acids Res.* **2020**, *48* (6), 3014−3028.
(110) Sambrook, J.; Fritsch, E. F.; Maniatis, T. *Molecular Cloning: A Lab Manual*. Cold Spring Harbor Press: Cold Spring Harbor, NY, 1989.
(111) Giusti, W. G.; Adriano, T. Synthesis and characterization of 5′-fluorescent-dye-labeled oligonucleotides. *Genome Res.* **1993**, *2* (3), 223−227.
(112) Studzińska, S.; Buszewski, B. Evaluation of ultra high-performance [corrected] liquid chromatography columns for the analysis of unmodified and antisense oligonucleotides. *Anal. Bioanal. Chem.* **2014**, *406* (28), 7127−36.

https://doi.org/10.1021/acsomega.2c05736
ACS Omega 2022, 7, 36888−36901